Macromolecules
COMMUNICATION TO THE EDITOR

Macromolecules **2010**, *43*, 7895–7899 **7895**
DOI: 10.1021/ma101697m

Tuning Polythiophene Crystallization through Systematic Side Chain Functionalization

Victor Ho, Bryan W. Boudouris, and Rachel A. Segalman*

Department of Chemical and Biomolecular Engineering, University of California, Berkeley, California 94720 and Materials Science Division, Lawrence Berkeley National Laboratory

Received July 27, 2010
Revised Manuscript Received August 28, 2010

Introduction. Poly(3-alkylthiophenes) (P3ATs) have been used broadly in organic electronic applications because they transport holes well ($\mu_h \sim 10^{-2}$ cm^2 V^{-1} s^{-1}), they are processable into thin films from many common organic solvents, and they have relatively low bandgaps ($E_g \sim 1.9$ eV) that can be tuned through chemical modification.[1−4] Originally introduced to increase solubility in polythiophenes, side chain alkyl substitutions allowed for synthesis of higher molecular weight polymers.[5,6] Since these initial efforts, side chain substitution has been used to tune the electronic properties of polythiophene,[7−9] improve polythiophene solubility in polar solvents,[10,11] and promote polymer interaction with inorganic species.[12] Some of these early results showed that the crystalline melting temperature is suppressed with the use of longer alkyl side chains;[13,14] however, little work has been performed to passivate rod−rod intermolecular interactions for control of nanoscale morphology. Poly(3-hexylthiophene) (P3HT) has become one of the most utilized active layer materials both in high performance organic field-effect transistors (OFETs)[15,16] and organic photovoltaic (OPV) devices.[17−19] However, it generally has not been possible to control the nucleation and growth of crystalline grains as the melting temperature of P3HT is extremely close to its degradation temperature.[20] To date, obtaining well-ordered morphologies over long ranges in P3HT thin films has proven difficult due to the rapid formation of thin lamellae (nanofibrils) when cast from solution[21−23] or cooling from the melt.[24] These strong rod−rod interactions also severely complicate phase behavior in multicomponent P3HT-containing systems, such as polymer-fullerene blends for OPV active layers.[25−28] Additionally, strong rod−rod interactions dominate the microphase separation in P3HT-containing block copolymers and prevent the formation of well-ordered domains commonly observed in all-coil block copolymers.[29−32] In fact, if passivation of rod self-alignment occurred, many previously unexplored microstructures could be found in P3AT-based block copolymers.

Recently, poly(3-alkylthiophene) copolymers have been synthesized in attempt to design polymer systems with controlled morphologies. Several groups have incorporated unsubstituted thiophene units randomly during polymerization to decrease the crystallization and control the morphology of blends and block copolymers.[33−36] Though nominally successful, this approach creates low crystallinity rod blocks caused by the random lattice defects introduced along the chain and decreases the optoelectronic properties of the polythiophene copolymers. Additionally, the Jenekhe group has copolymerized 3-alkylthiophenes with octyl and butyl side chains resulting in semicrystalline polymers with thermal properties that can be tuned by changing the feed ratio of monomers.[37,38] Though these random copolymers exhibited improved photovoltaic efficiencies relative to either homopolymer,[39] thermal properties of the copolymers were limited by those of the constituent homopolymers and transition temperatures were found to vary linearly between those of the pure components. Systematic side chain substitution provides a convenient synthetic approach to controlling the rod−rod interactions of polythiophenes in order to obtain a chemically well-defined, semicrystalline polymer with distinct thermal transitions.

Here we detail the thermal, structural, and electronic properties of a less-studied P3AT, poly(3-(2′-ethyl)hexylthiophene) (P3EHT). We compare its properties to two more common P3ATs, poly(3-hexylthiophene) and poly(3-dodecylthiophene) (P3DDT). Three different molecular weights of each type of polymer were synthesized, and the molecular weights were controlled such that the average number of thiophene repeat units per chain was approximately the same between the P3HT, P3DDT, and P3EHT series. We show that P3DDT and P3EHT, with melting transitions sufficiently removed from the thermal degradation temperature, exhibit a nematic liquid crystalline phase, observed by polarized optical microscopy (POM), with a molecular weight-dependent nematic−isotropic transition temperature. From the nematic−isotropic transition temperatures, the Maier−Saupé interaction parameter has been extracted for P3DDT and P3EHT, which quantitatively shows the significantly reduced rod−rod interactions in P3EHT. The bulk and thin film microstructure of the polymers were studied using wide-angle X-ray scattering (WAXS) and atomic force microscopy (AFM), respectively. Additionally, the optoelectronic properties of these materials are studied using thin film ultraviolet−visible (UV−vis) absorption spectroscopy and field-effect transistor (FET) testbeds. These results demonstrate that P3EHT has comparable optical and charge transport properties to that of P3HT and P3DDT. Importantly, the introduction of a short branch in the hexyl side chain causes P3EHT to have a lower melting temperature, lower liquid crystalline transition temperature, and reduced rod−rod interactions. These assets, combined with similar optoelectronic properties to that of P3HT, will allow for a better understanding of crucial structure−property relationships in P3AT-containing systems and offer researchers another handle with which to control the assembly of these polymers.

Results and Discussion. Regioregular (> 98% head-to-tail coupling), low polydispersity P3ATs were prepared using the Grignard metathesis (GRIM) method developed by the McCullough group (Scheme S1).[40,41] Three samples of each substituted P3AT were synthesized and their properties are summarized in Table 1. The polymer molecular weights and regioregularities were determined by ^{1}H NMR analysis and size exclusion chromatography (SEC) against polystyrene standards was used to ascertain the polydispersity index (PDI) values. Molecular weights were controlled so that the number of thiophene repeat units is approximately matched across all three polymer series.

*To whom correspondence should be addressed. E-mail: segalman@berkeley.edu.

Published on Web 09/15/2010

Table 1. Characterization of P3AT Samples

sample[a]	N^b	$M_w/M_n{}^c$	$T_m{}^d$ (°C)	$d_{010}{}^f$ (nm)	FET Mobility[g] ($cm^2\ V^{-1}\ s^{-1}$)
P3HT-43	43	1.1	224	0.38	1.6×10^{-3}
P3HT-55	55	1.1	234	0.37	2.8×10^{-3}
P3HT-73	73	1.1	236	0.38	1.3×10^{-3}
P3DDT-30	30	1.3	157	0.39	4.6×10^{-4}
P3DDT-50	50	1.2	164	0.39	8.1×10^{-4}
P3DDT-79	79	1.2	169	0.39	6.5×10^{-4}
P3EHT-37	37	1.2	68, 78[e]	0.41	3.2×10^{-5}
P3EHT-54	54	1.2	71, 83[e]	0.41	1.1×10^{-4}
P3EHT-65	65	1.2	76, 89[e]	0.41	1.2×10^{-4}

[a] P3AT-*X* indicates the polymer has an *X* average number of thiophene repeat units per chain. [b] As determined by ^{1}H NMR spectroscopy. [c] As determined by SEC versus polystyrene standards. [d] Main chain melting transition temperatures, as determined from the peak endothermic value of the DSC thermogram. [e] Two temperatures indicate two distinct peaks in the DSC data, suggesting the coexistence of two crystal forms (see text). [f] As determined by WAXS. [g] Average field-effect hole mobility values were calculated in the saturation regime ($V_D = -80$ V).

Differential scanning calorimetry (DSC) data (Figure 1a) show that the alkyl chain architecture has a significant effect on the melting transition temperature of the polymers. Thermograms for P3HT indicate that the main chain melting transitions occur over the range 224−236 °C, depending on the molecular weight of the polymer. When the number of alkyl groups in the side chain is increased from 6 to 12 in P3DDT, the melting transition decreases to between 157 and 169 °C. A broad secondary peak between 20 and 80 °C is consistent with previous literature reports of the melting of interdigitated dodecyl side chains.[42] Introducing the branched architecture of the 3-(2′-ethyl)hexyl side chain further depresses the main chain melting transition temperature. When annealed at temperatures below the melting transition temperature for at least an hour, P3EHT shows two distinct peaks between 70 and 90 °C, characteristic of the existence of two coexisting semicrystalline microstructures.[43,44] We note the presence of two melting endotherms in the P3HT and P3DDT thermograms as well; however, these are not as pronounced as the P3EHT samples and appear as small shoulders of the main peaks. Side chain crystallization is not expected due, in part, to the irregular geometry imparted by the stereocenter at the 2-carbon of the hexyl side chain. It should be noted that if P3EHT is not allowed sufficient time to crystallize (for example if a film is cast directly from solvent or a powder is measured immediately after drying from solvent), no melting is observed, suggesting that this polymer has relatively slow crystallization kinetics. Therefore, reports of the thermal transitions of P3EHT are highly dependent on thermal history.[45]

Because the melting temperatures of P3DDT and P3EHT are removed far from the degradation temperatures of these polymers, they exhibit interesting liquid crystalline behavior at temperatures greater than their respective melting temperatures. Polarized optical microscopy (POM) was used to identify these liquid crystalline phases via their well-known birefringent behavior.[46,47] These phases arise because rodlike molecules tend to align in the melt due to geometric constraints arising from the anisotropic shape of the molecules. In particular, the nematic phase, in which molecules of a crystal grain preferentially align along a given rod director, is evidenced by schlieren textures which originate from orientational point defects.[48] Because of high viscosity inherent to polymer melts, nematic textures tend to be small scale and can be enlarged by shearing (by sliding the top slide of a microscope slide-polymer-microscope slide sandwich) to a length scale observable by optical microscopy. The inset of

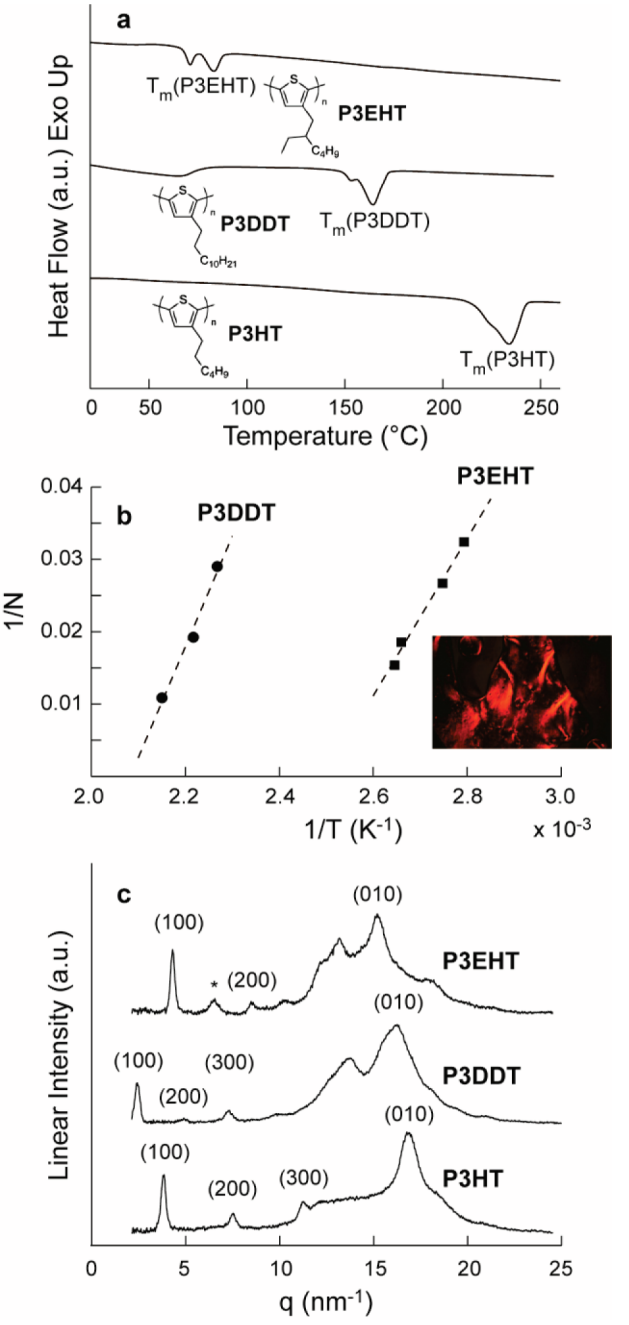

Figure 1. (a) DSC thermograms of representative P3HT, P3DDT, and P3EHT polymers at a heating rate of 10 °C/min. The chemical structures of the three polymers are inset in the figure. (b) Inverse P3AT chain length as a function of the inverse nematic−isotropic transition temperature for P3DDT (circles) and P3EHT (squares). The slopes of linear fits to the data (dashed lines) are related to the Maier−Saupé rod−rod interaction parameter for the respective polymers. The inset shows a POM image of a representative P3EHT polymer in the nematic phase. The image was taken at 10× magnification after gentle shearing. (c) WAXS powder diffraction patterns for representative P3HT, P3DDT, and P3EHT. The prominent lamellae reflections are labeled as (*h*00) and the $\pi-\pi$ stacking distance is labeled as (010). The reflection labeled with ∗ is consistent with the presence of a second crystal structure present in the P3EHT sample, as seen in DSC.

Figure 1b shows the presence of a nematic phase in a representative sample of P3EHT upon shearing in the melt. Nematic phases are observed in P3HT and P3DDT, as well, and similar schlieren patterns are formed upon shearing above the melting temperature. On slow heating, the patterns persist until the nematic−isotropic transition, at which point

an isotropic phase is obtained and the sample loses birefringent textures.

The Maier−Saupé parameter can be used to quantify the attraction between rods and is useful in understanding the relative strengths of the alignment interactions in these polymers.[47,49] Rod−rod interaction parameters for P3DDT and P3EHT were extracted by performing linear regressions on the observed nematic−isotropic transition temperatures over a range of molecular weights[50] (Figure 1b), following the procedure described in previous work.[51] Although a nematic phase is present in P3HT, a nematic−isotropic transition is precluded by thermal degradation; as a result its Maier−Saupé parameter is undefined. P3DDT and P3EHT Maier−Saupé parameters are $\mu_{P3DDT} = 153T^{-1} - 0.3$ and $\mu_{P3EHT} = 109T^{-1} - 0.3$; this suggests that the presence of the alkyl branch in the P3EHT side chain results in a decrease in interaction strength of approximately 33% relative to P3DDT.

While P3EHT has minimized rod−rod interactions and a depressed melting transition, its crystalline structure, as determined by powder wide-angle X-ray scattering (WAXS), was strikingly similar to that of P3HT.[52] The unit cells for P3HT and P3DDT have been presented in literature as orthorhombic cells with observable reflections from backbone spacing and $\pi-\pi$ stacking.[23,53,54] The (100) reflection of P3HT, which measures distance between backbones across alkyl chains, is present at 3.84 nm^{-1}, corresponding to a lattice spacing of 1.64 nm; peaks consistent with the (200) and (300) reflections are present also. The (010) reflection, measuring the spacing of $\pi-\pi$ stacking between thiophene rings, can be seen as a broad hump with a distinct peak at 16.65 nm^{-1}. As expected, P3DDT patterns show (100), (200), and (300) peaks at 2.47, 4.93, 7.27 nm^{-1} at larger domain spacings than those in P3HT patterns due to the longer side chain; a peak at 16.18 nm^{-1}, which corresponds to the (010) plane is consistent with the $\pi-\pi$ stacking distance reported in the literature.[53−55] Powder WAXS patterns (Figure 1c) demonstrate that P3EHT is semicrystalline, similar to the other polythiophene derivatives, and has a similar packing motif as that of P3HT and P3DDT, but with slightly different lattice spacing. We note the presence of the peak labeled ∗ at q-values between the (100) and (200) planes in the P3EHT samples. This may be indicative of a second P3EHT crystal structure, as samples with multiple polymorphic phases have been observed in other P3ATs.[44,56] The (100) reflection of P3EHT is located at 4.29 nm^{-1}, which indicates a slightly smaller lattice spacing than in P3HT. However, the (010) reflections are shifted to a slightly lower q-value relative to both P3DDT and P3HT with a $\pi-\pi$ spacing of 0.41 nm. Furthermore, the greater sharpness of this diffraction pattern is suggestive that the smaller undercooling temperatures possible in this low melting system result in larger grain size.

Tapping mode atomic force microscopy (AFM) images show the semicrystalline nature of the P3ATs in as-spun thin films, evidenced by the presence of a percolating network of nanofibrils (Figure 2).[22] In representative images, fibrils in P3HT-55 (Figure 2a) and P3EHT-37 (Figure 2b) have widths of ∼32 nm and ∼15 nm, respectively. Interestingly, the lengths of the P3HT nanowires are dramatically longer than in the P3EHT case. This difference in nanofibril length between P3ATs may affect the in-plane charge transport in these materials.

Despite the slightly larger $\pi-\pi$ packing distance of P3EHT (relative to P3HT) the optoelectronic properties are comparable, as evidenced by UV−vis light absorption spectroscopy and field-effect transistor (FET) mobilities. As shown in Figure 3a, the global maximum absorbance values for P3HT and P3DDT solutions in chloroform are located at

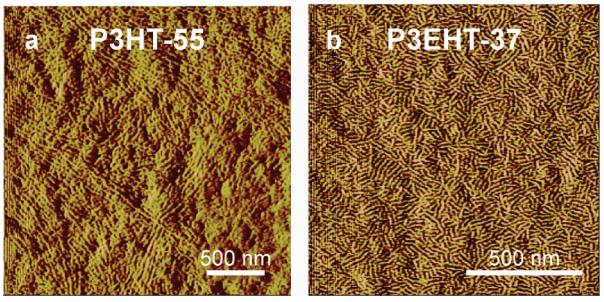

Figure 2. Atomic force microscopy tapping mode images of (a) P3HT-55 and (b) P3EHT-37 as-spun thin films showing the nanofibril microstructures present in both P3AT materials. Note that the lengths of the fibers in the P3HT sample are longer than in the P3EHT sample. Films were fabricated by spin-coating a 10 mg of polymer per 1 mL of chloroform solution at 1000 rpm for 1 min onto a silicon dioxide substrate. Final thin film thicknesses were ∼80 nm as measured by profilometry.

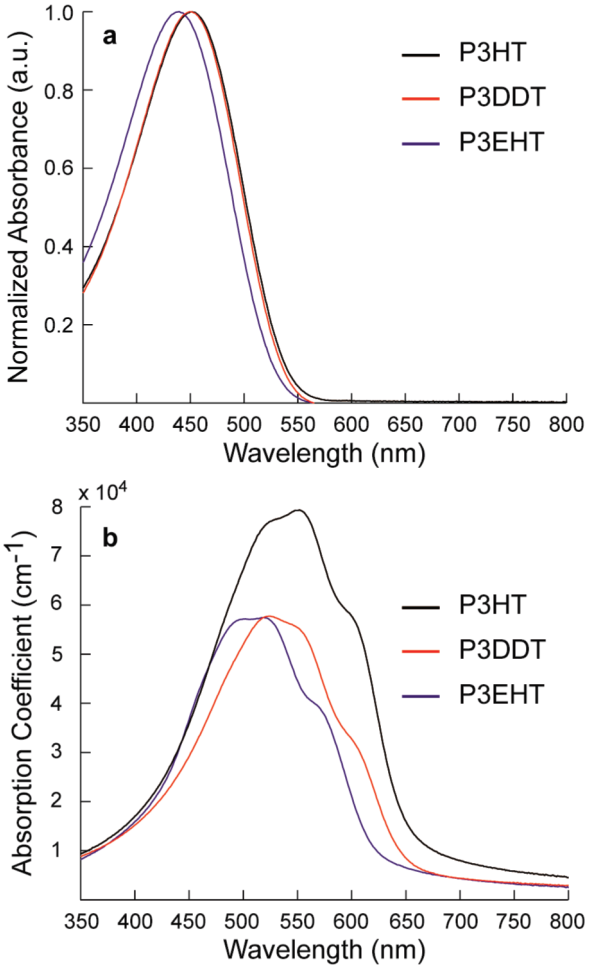

Figure 3. UV−vis light absorption profiles of P3HT (black), P3DDT (red), and P3EHT (blue) (a) in chloroform solutions and (b) cast as thin films. The solution concentration was 10 μg of polymer per 1 mL of chloroform. Thin films were fabricated by spin-coating from 10 mg of polymer per 1 mL of chloroform solutions at 2000 rpm for 1 min onto a glass substrate. All film thicknesses were ∼60 nm, as measured by profilometry.

450 nm while the P3EHT maximum is slightly blue-shifted to 440 nm. This suggests that the branched alkyl chain architecture in P3EHT may introduce slight twists in the thiophene backbone, which occasionally disrupt conjugation.[57,58] Upon casting into thin films from chloroform the UV−vis spectra of all the P3ATs were red-shifted and a vibronic shoulder became

evident at lower energies (Figure 3b). The thin film absorption profiles for P3DDT and P3HT (Figure 3b) are identical, except that P3HT has a larger maximum absorption coefficient, consistent with previous reports.[24,33] P3EHT also shows a similar profile with an almost identical maximum absorption coefficient as P3DDT. However, the vibronic shoulder for P3EHT is blue-shifted 30 nm, suggesting a decrease in the conjugation length in the solid state; this causes the optical bandgap of P3EHT to be ~0.1 eV greater than the bandgaps of P3HT and P3DDT. While not identical, the solid state absorption profiles obtained for P3EHT are very similar to those of P3HT and P3DDT.

Charge transport in these materials was compared by fabricating top contact, bottom gate FETs with each of the polymers as the active layer, as summarized in Table 1. P3HT FETs exhibited hole mobilities of $\mu_h \sim 10^{-3}$ cm^2 V^{-1} s^{-1}, while P3DDT showed mobilities which were 1 order of magnitude lower on average, consistent with previous reports for relatively low molecular weight[59] P3HT and P3DDT. The hole mobility of P3DDT has been seen to be lower than P3HT due to the larger lattice spacing in both the (100) and (010) directions.[60] P3EHT showed similar hole mobilities to those of P3DDT polymers ($\mu_h \sim 10^{-4}$ cm^2 V^{-1} s^{-1}). Relative to P3HT, P3EHT has similar (100) spacing to P3HT, but a slightly larger $\pi-\pi$-stacking distance (~0.03 nm). Therefore, it is expected that the overall mobility of P3EHT would be slightly lower relative to P3HT. It is surprising, however, to note that the incorporation of the bulkier, branched side chain and resultant increased (010) spacing does not appear much more detrimental to the field-effect mobility than increasing the straight chain length from 6 to 12 carbons in P3DDT. Given that P3DDT previously has been demonstrated to have practical properties in both transistor and photovoltaic devices, these results suggest that P3EHT also will be a potentially useful organic electronic active layer material.

Conclusions. Straight and branched side chain P3ATs with narrow molecular weight distributions have been synthesized using the GRIM method. DSC, powder WAXS, and AFM confirm that P3EHT is a semicrystalline polymer, similar to P3HT and P3DDT; a fact which can be overlooked if relying solely on DSC data acquired at a fast heating rate. The lower melting transitions for P3DDT and P3EHT allow for observation of a liquid crystalline region which is unstable in P3HT due to the proximity of its melting temperature to thermal degradation. The Maier−Saupé rod−rod interaction parameter for P3DDT and P3EHT were determined and the Maier−Saupé parameter for P3DDT was found to be significantly higher than P3EHT, suggesting a larger strength of rod−rod interactions. Powder WAXS spectra showed lattice spacings which vary with the length and architecture of the alkyl side chain. Introducing a branch in the P3EHT case slightly increases the (010) spacing relative to the P3HT and P3DDT cases. UV−vis absorbance spectroscopy and FET mobility measurements demonstrate that P3EHT has similar optoelectronic properties to P3HT and P3DDT. These facts, coupled with the unique thermal and liquid crystalline properties of P3EHT, makes poly(3-(2′-ethyl)-hexylthiophene) a promising material for higher order microstructural control in pristine P3AT films, P3AT-containing blends, and P3AT-based block copolymers that can be readily utilized in organic electronic devices.

Acknowledgment. We gratefully acknowledge support through an NSF CAREER award for the synthesis and characterization of structure and support through the DOE-Office of Science Plastic Electronics Program at Lawrence Berkeley National Laboratories for device fabrication and characterization. VH gratefully acknowledges the National Science Foundation for a graduate fellowship. Device fabrication and characterization was performed at the Molecular Foundry, a Lawrence Berkeley National Laboratory user facility supported by the Office of Science, Office of Basic Energy Sciences, U.S. Department of Energy, under Contract No. DE-AC02-05CH11231.

Supporting Information Available: Text giving detailed synthetic procedures and experimental techniques, a scheme showing the synthesis of P3ATs, and a figure showing representative field-effect transistor data. This material is available free of charge via the Internet at http://pubs.acs.org.

References and Notes

(1) McCullough, R. D. *Adv. Mater.* **1998**, *10*, 93–116.
(2) Osaka, I.; McCullough, R. D. *Acc. Chem. Res.* **2008**, *41*, 1202–1214.
(3) Thompson, B. C.; Fréchet, J. M. J. *Angew. Chem., Int. Ed.* **2008**, *47*, 58–77.
(4) Peet, J.; Heeger, A. J.; Bazan, G. C. *Acc. Chem. Res.* **2009**, *42*, 1700–1708.
(5) Elsenbaumer, R. L.; Jen, K. Y.; Oboodi, R. *Synth. Met.* **1986**, *15*, 169–174.
(6) Jen, K. Y.; Miller, G. G.; Elsenbaumer, R. L. *J. Chem. Soc., Chem. Commun.* **1986**, 1346–1347.
(7) McCullough, R. D.; Williams, S. P. *J. Am. Chem. Soc.* **1993**, *115*, 11608–11609.
(8) Ogawa, K.; Stafford, J. A.; Rothstein, S. D.; Tallman, D. E.; Rasmussen, S. C. *Synth. Met.* **2005**, *152*, 137–140.
(9) Hou, J. H.; Chen, T. L.; Zhang, S. Q.; Huo, L. J.; Sista, S.; Yang, Y. *Macromolecules* **2009**, *42*, 9217–9219.
(10) McCullough, R. D.; Ewbank, P. C.; Loewe, R. S. *J. Am. Chem. Soc.* **1997**, *119*, 633–634.
(11) Viinikanoja, A.; Areva, S.; Kocharova, N.; Aaritalo, T.; Vuorinen, M.; Savunen, A.; Kankare, J.; Lukkari, J. *Langmuir* **2006**, *22*, 6078–6086.
(12) Liu, J. S.; Kadnikova, E. N.; Liu, Y. X.; McGehee, M. D.; Fréchet, J. M. J. *J. Am. Chem. Soc.* **2004**, *126*, 9486–9487.
(13) Zhao, Y.; Keroack, D.; Yuan, G. X.; Massicotte, A.; Hanna, R.; Leclerc, M. *Macromol. Chem. Phys.* **1997**, *198*, 1035–1049.
(14) Malik, S.; Nandi, A. K. *J. Polym. Sci., Part B: Polym. Phys.* **2002**, *40*, 2073–2085.
(15) Sirringhaus, H.; Brown, P. J.; Friend, R. H.; Nielsen, M. M.; Bechgaard, K.; Langeveld-Voss, B. M. W.; Spiering, A. J. H.; Janssen, R. A. J.; Meijer, E. W.; Herwig, P.; de Leeuw, D. M. *Nature* **1999**, *401*, 685–688.
(16) Wang, G. M.; Swensen, J.; Moses, D.; Heeger, A. J. *J. Appl. Phys.* **2003**, *93*, 6137–6141.
(17) Padinger, F.; Rittberger, R. S.; Sariciftci, N. S. *Adv. Funct. Mater.* **2003**, *13*, 85–88.
(18) Li, G.; Shrotriya, V.; Huang, J. S.; Yao, Y.; Moriarty, T.; Emery, K.; Yang, Y. *Nat. Mater.* **2005**, *4*, 864–868.
(19) Ma, W. L.; Yang, C. Y.; Gong, X.; Lee, K.; Heeger, A. J. *Adv. Funct. Mater.* **2005**, *15*, 1617–1622.
(20) Kuila, B. K.; Nandi, A. K. *J. Phys. Chem. B* **2006**, *110*, 1621–1631.
(21) Liu, J. S.; Sheina, E.; Kowalewski, T.; McCullough, R. D. *Angew. Chem., Int. Ed.* **2001**, *41*, 329–332.
(22) Zhang, R.; Li, B.; Iovu, M. C.; Jeffries-EL, M.; Sauve, G.; Cooper, J.; Jia, S. J.; Tristram-Nagle, S.; Smilgies, D. M.; Lambeth, D. N.; McCullough, R. D.; Kowalewski, T. *J. Am. Chem. Soc.* **2006**, *128*, 3480–3481.
(23) Wu, Z. Y.; Petzold, A.; Henze, T.; Thurn-Albrecht, T.; Lohwasser, R. H.; Sommer, M.; Thelakkat, M. *Macromolecules* **2010**, *43*, 4646–4653.
(24) Boudouris, B. W.; Molins, F.; Blank, D. A.; Frisbie, C. D.; Hillmyer, M. A. *Macromolecules* **2009**, *42*, 4118–4126.
(25) Müller, C.; Ferenczi, T. A. M.; Campoy-Quiles, M.; Frost, J. M.; Bradley, D. D. C.; Smith, P.; Stingelin-Stutzmann, N.; Nelson, J. *Adv. Mater.* **2008**, *20*, 3510–3511.
(26) van Bavel, S.; Sourty, E.; de With, G.; Frolic, K.; Loos, J. *Macromolecules* **2009**, *42*, 7396–7403.
(27) Chen, L. M.; Hong, Z. R.; Li, G.; Yang, Y. *Adv. Mater.* **2009**, *21*, 1434–1449.
(28) Beal, R. M.; Stavrinadis, A.; Warner, J. H.; Smith, J. M.; Assender, H. E.; Watt, A. A. R. *Macromolecules* **2010**, *43*, 2343–2348.

(29) Olsen, B. D.; Segalman, R. A. *Mat. Sci. Eng. R-Rep.* **2008**, *62*, 37–66.
(30) Segalman, R. A.; McCulloch, B.; Kirmayer, S.; Urban, J. J. *Macromolecules* **2009**, *42*, 9205–9216.
(31) Botiz, I.; Darling, S. B. *Mater. Today* **2010**, *13*, 42–51.
(32) Darling, S. B. *Energy Environ. Sci.* **2009**, *2*, 1266–1273.
(33) Thompson, B. C.; Kim, B. J.; Kavulak, D. F.; Sivula, K.; Mauldin, C.; Fréchet, J. M. J. *Macromolecules* **2007**, *40*, 7425–7428.
(34) Boudouris, B. W.; Frisbie, C. D.; Hillmyer, M. A. *Macromolecules* **2010**, *43*, 3566–3569.
(35) Wu, P.-T.; Ren, G. Q.; Kim, F. S.; Li, C. X.; Mezzenga, R.; Jenekhe, S. A. *J. Polym. Sci., Part A: Polym. Chem.* **2010**, *48*, 614–626.
(36) Hollinger, J.; Jahnke, A. A.; Coombs, N.; Seferos, D. S. *J. Am. Chem. Soc.* **2010**, *132*, 8546–8547.
(37) Wu, P.-T.; Ren, G.; Li, C.; Mezzenga, R.; Jenekhe, S. A. *Macromolecules* **2009**, *42*, 2317–2320.
(38) Wu, P.-T.; Ren, G. Q.; Jenekhe, S. A. *Macromolecules* **2010**, *43*, 3306–3313.
(39) Ren, G.; Wu, P.-T.; Jenekhe, S. A. *Chem. Mater.* **2010**, *22*, 2020–2026.
(40) Loewe, R. S.; Khersonsky, S. M.; McCullough, R. D. *Adv. Mater.* **1999**, *11*, 250–251.
(41) Loewe, R. S.; Ewbank, P. C.; Liu, J.; Zhai, L.; McCullough, R. D. *Macromolecules* **2001**, *34*, 4324–4333.
(42) Liu, S. L.; Chung, T. S. *Polymer* **2000**, *41*, 2781–2793.
(43) Prosa, T. J.; Winokur, M. J.; Moulton, J.; Smith, P.; Heeger, A. J. *Macromolecules* **1992**, *25*, 4364–4372.
(44) Prosa, T. J.; Winokur, M. J.; McCullough, R. D. *Macromolecules* **1996**, *29*, 3654–3656.
(45) Zhang, Y.; Tajima, K.; Hirota, K.; Hashimoto, K. *J. Am. Chem. Soc.* **2008**, *130*, 7812–7813.
(46) Chandrasekhar, S. *Liquid crystals*, 2nd ed.; Cambridge University Press: Cambridge,England, and New York, 1992.
(47) Olsen, B. D.; Segalman, R. A. *Macromolecules* **2005**, *38*, 10127–10137.
(48) Wang, X. J.; Zhou, Q. F. *Liquid Crystalline Polymers*; World Scientific Publishing Company, Incorporated: Singapore, 2004.
(49) Olsen, B. D.; Segalman, R. A. *Macromolecules* **2006**, *39*, 7078–7083.
(50) Note that for high molecular weights a divergence from the expected linear behavior is observed, presumably because chains are entangled and lack necessary mobility to reach the desired equilibrium state on an experimentally convenient time scale. Therefore, only chains which were sufficiently short to maintain linear behavior were used in compiling Figure 1b.
(51) Olsen, B. D.; Jang, S. Y.; Luning, J. M.; Segalman, R. A. *Macromolecules* **2006**, *39*, 4469–4479.
(52) Note that no dependence of molecular weight on lattice spacing was observed for any of the polymers investigated.
(53) Prosa, T. J.; Moulton, J.; Heeger, A. J.; Winokur, M. J. *Macromolecules* **1999**, *32*, 4000–4009.
(54) Causin, V.; Marega, C.; Marigo, A.; Valentini, L.; Kenny, J. M. *Macromolecules* **2005**, *38*, 409–415.
(55) Boudouris, B. W.; Frisbie, C. D.; Hillmyer, M. A. *Macromolecules* **2008**, *41*, 67–75.
(56) Arroyo-Villan, M. I.; Diaz-Quijada, G. A.; Abdou, M. S. A.; Holdcroft, S. *Macromolecules* **1995**, *28*, 975–984.
(57) Baughman, R. H.; Chance, R. R. *J. Appl. Phys.* **1976**, *47*, 4295–4300.
(58) Tashiro, K.; Ono, K.; Minagawa, Y.; Kobayashi, M.; Kawai, T.; Yoshino, K. *J. Polym. Sci., Part B: Polym. Phys.* **1991**, *29*, 1223–1233.
(59) Kline, R. J.; McGehee, M. D.; Kadnikova, E. N.; Liu, J.; Fréchet, J. M. J.; Toney, M. F. *Macromolecules* **2005**, *38*, 3312–3319.
(60) Babel, A.; Jenekhe, S. A. *Synth. Met.* **2005**, *148*, 169–173.